Kinetic Mechanism of Folding and Unfolding of Rhodobacter capsulatus Cytochrome c 2 †

ARTICLE *in* BIOCHEMISTRY · JANUARY 1997

Impact Factor: 3.02 · DOI: 10.1021/bi961976k · Source: PubMed

3 AUTHORS, INCLUDING:

J. Michael Sauder
Eli Lilly
63 PUBLICATIONS **2,391** CITATIONS
SEE PROFILE

Heinrich Roder
Fox Chase Cancer Center
121 PUBLICATIONS **8,484** CITATIONS
SEE PROFILE

Kinetic Mechanism of Folding and Unfolding of *Rhodobacter capsulatus* Cytochrome c_2[†]

J. Michael Sauder,[‡,§] Neil E. MacKenzie,[∥] and Heinrich Roder*[,‡,§]

Institute for Cancer Research, Fox Chase Cancer Center, 7701 Burholme Avenue, Philadelphia, Pennsylvania 19111, Department of Biochemistry and Biophysics, University of Pennsylvania, Philadelphia, Pennsylvania 19104-6059, and Department of Pharmaceutical Sciences, College of Pharmacy, University of Arizona, Tucson, Arizona 85721

Received August 7, 1996; Revised Manuscript Received October 8, 1996[⊗]

ABSTRACT: In spite of marginal sequence homology, cytochrome c_2 from photosynthetic bacteria and the mitochondrial cytochromes *c* exhibit some striking structural similarities, including the tertiary arrangement of the three main helices. To compare the folding mechanisms for these two distantly related groups of proteins, equilibrium and kinetic measurements of the folding/unfolding reaction of cytochrome c_2 from *Rhodobacter capsulatus* were performed as a function of guanidine hydrochloride (GuHCl) concentration in the absence and presence of a stabilizing salt, sodium sulfate. Quenching of the fluorescence of Trp67 by the heme was used as a conformational probe. Kinetic complexities due to non-native histidine ligation are avoided, since cytochrome c_2 contains only one histidine, His17, which forms the axial heme ligand under native and denaturing conditions. Quantitative kinetic modeling showed that both equilibrium and kinetic results are consistent with a minimal four-state mechanism with two sequential intermediates. The observation of a large decrease in fluorescence during the 2-ms dead-time of the stopped-flow measurement (burst phase) at low GuHCl concentration, followed by a sigmoidal recovery of the initial amplitude toward the unfolding transition region, is attributed to a well-populated compact folding intermediate in rapid exchange with unfolded molecules. A nearly denaturant-independent process at *low* GuHCl concentrations reflects the rate-limiting conversion of a compact intermediate to the native state. At *high* GuHCl concentrations, a process with little denaturant dependence is attributed to the rate-limiting Met96−iron deligation process during unfolding, which is supported by the kinetics of imidazole binding. The strong GuHCl-dependence of folding and unfolding rates near the midpoint of the equilibrium transition is attributed to destabilization of each intermediate and their transition states in folding and unfolding. Addition of sodium sulfate shifts the rate profile to higher denaturant concentration, which can be understood in terms of the relative stabilizing effect of the salt on partially and fully folded states.

The class I *c*-type cytochromes are a large family of heme proteins that act as electron carriers in respiratory and photosynthetic pathways (Meyer & Kamen, 1982; Mathews, 1985; Moore & Pettigrew, 1990). With well over 100 known amino acid sequences for species ranging from bacteria through mammals and crystal structures for about a dozen representative members, the cytochromes *c* are among the best characterized small monomeric proteins. Thus, they are ideally suited for comparative studies of protein structure, folding, and stability. Whereas the mitochondrial cytochromes *c* are highly conserved, their bacterial homologues, the cytochromes c_2, are a structurally and functionally more diverse group of proteins (Salemme, 1977). Aside from a number of functionally important residues, including a Cys-X-X-Cys-His motif near the N-terminus and a Met in the C-terminal half involved in heme attachment and ligation, as well as a few additional residues involved in heme contacts and interactions with the axial ligands, there is only limited sequence identity between the mitochondrial and the bacterial proteins. Nevertheless, they share some common structural motifs, including the pair of N- and C-terminal α-helices involved in a tight orthogonal packing arrangement (cf. Figure 1) and a third helix adjacent to the methionine ligand, which together provide most of the hydrophobic contacts with the heme (Chothia & Lesk, 1985). Other regions of the structure consisting of irregular loops and two additional helices show a larger degree of variability.

Previous studies on the kinetic mechanism of folding and unfolding have been limited to a few mitochondrial cytochromes *c*, including the two isoforms from yeast (Nall & Landers, 1981; Zuniga & Nall, 1983) and horse cytochrome *c* [reviewed in Roder and Elöve (1994)], which has been the subject of numerous kinetic studies over the past 25 years (Babul & Stellwagen, 1972; Ikai et al., 1973; Tsong, 1973; Ridge et al., 1981; Dyson & Beattie, 1982; Brems & Stellwagen, 1983; Roder et al., 1988; Elöve et al., 1992, 1994; Pryse et al., 1992; Sosnick et al., 1994; Colón et al., 1996). Earlier kinetic studies on horse cytochrome *c*, based on optical probes and hydrogen exchange labeling methods, revealed a complex folding mechanism with multiple path-

[†] This work was supported by NIH Grant GM35926 and NSF Grant MCB 9306367 to H.R., and by NIH Grant CA06927 and an appropriation from the Commonwealth of Pennsylvania to the Institute for Cancer Research.

* Correspondence should be addressed to this author at the Fox Chase Cancer Center. Phone: (215) 728-3123. FAX: (215) 728-3574. E-mail: H_Roder@fccc.edu.

[‡] Fox Chase Cancer Center.

[§] University of Pennsylvania.

[∥] University of Arizona.

[⊗] Abstract published in *Advance ACS Abstracts,* December 15, 1996.

S0006-2960(96)01976-9 CCC: $12.00

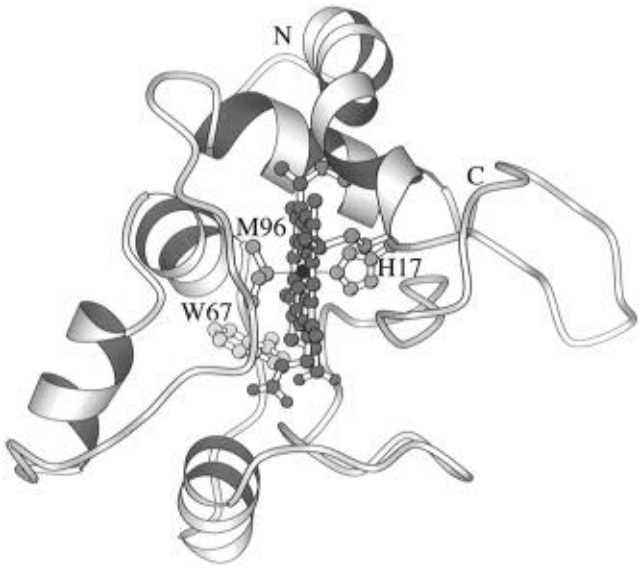

FIGURE 1: Ribbon diagram of the structure of *Rhodobacter capsulatus* cytochrome c_2 based on the crystal structure (1C2R) of Benning et al. (1991). Cyt c_2 has only one histidine and one methionine, which serve as axial ligands to the heme iron, and a single tryptophan, which serves as a fluorescence probe. This figure was prepared with MolScript 1.4 (Kraulis, 1991).

ways and several intermediates, including a collapsed state with native-like secondary structure formed within the 2-ms dead-time of the stopped-flow experiment (Elöve et al., 1992), followed by formation of a partially structured intermediate with interacting N- and C-terminal helices (I_{NC}) on the 10-ms time scale (Roder et al., 1988). It has been shown that a normally unligated histidine (His26 or His33), when deprotonated, can replace the Met80 heme ligand under denaturing conditions (Elöve & Roder, 1991; Elöve et al., 1994; Sosnick et al., 1994) and act as a kinetic trap during folding, which allows accumulation of the structural intermediate I_{NC}. Dissociation of the non-native ligand at a rate of about 3 s^{-1} is the rate-limiting step in folding at neutral pH, while the 10-ms process (formation of I_{NC}) directly leads to the native state at lower pH.

We report here the first kinetic folding studies on a bacterial *c*-type cytochrome, the cytochrome c_2 isolated from the photosynthetic bacterium *Rhodobacter capsulatus*.[1] The function and stability of this protein have been studied extensively by protein engineering methods (Daldal et al., 1986; Caffrey & Cusanovich, 1991a,b, 1993; Caffrey et al., 1992). Efficient expression of cyt c_2 in its natural host also facilitated homo- and heteronuclear NMR studies of its structure and dynamics (Gooley et al., 1990, 1991a,b, 1992; Gooley & MacKenzie, 1990). Crystallographic analysis of this 116-residue protein (Benning et al., 1991) revealed close structural similarities with other bacterial cytochromes c_2 (Salemme et al., 1973; Timkovich & Dickerson, 1976; Ambler et al., 1979). Comparison with the structure of horse cytochrome *c* (Bushnell et al., 1990) shows a similar packing arrangement for three of the five helical segments (those on top and to the left of the heme in Figure 1), although the N-terminal helix is distorted and has some 3_{10}-helical character and the C-terminal helix is shorter than the corresponding helix in the horse protein. The two remaining helices (residues 55−63 and 80−87) are significantly longer than their homologues in horse cytochrome *c*. The heme environment, including the detailed geometry of the axial ligands (His17 and Met96 in cyt c_2), is well conserved between the cytochromes *c* from *Rb. capsulatus* and horse (Benning et al., 1991). Moreover, both proteins have a single tryptophan (Trp67 in cyt c_2 and Trp59 in horse cyt *c*) located in homologous positions in contact with the heme (Figure 1), which serves as a convenient fluorescence probe to monitor structural collapse during folding. Mutagenesis studies in *Rb. capsulatus* suggest that this highly conserved tryptophan primarily serves a structural rather than a functional role (Caffrey & Cusanovich, 1993).

Shakhnovich et al. (1996) recently predicted that residues involved in critical interactions in the transition state for folding should be conserved in evolution. One difficulty in comparing the protein folding mechanisms for natural variants is that the kinetics of folding are often dominated by extraneous factors, such as isomerization of prolyl peptide bonds and, in the case of metalloproteins, changes in ligation state. These intrinsically slow events can become rate-limiting during folding and obscure the underlying structural transitions. An attractive feature of cyt c_2 is that its native axial heme ligands, His17 and Met97, are the only histidine and methionine residues in the protein. Because of the covalent constraints due to the adjacent heme attachment, His17 remains bound to the heme iron under typical denaturing conditions. Although the methionine sulfur ligand dissociates more readily, for example, at alkaline pH (Caffrey & Cusanovich, 1991b), there is no evidence that its formation becomes rate-limiting during folding. In contrast, horse cyt *c* contains two additional histidines and one additional methionine that can potentially undergo non-native interactions with the heme iron. Cyt c_2, therefore, provides an opportunity for studying cytochrome *c* folding in the absence of competing ligation events, especially at mildly acidic pH, where other potential iron ligands (e.g., side-chain amide, N-terminal amino, and tyrosine hydroxyl groups) are protonated. As a result, the kinetics of folding and unfolding of cyt c_2 discussed in this paper are less complex than those of the mitochondrial cytochromes *c*.

The kinetics of folding and unfolding of cyt c_2 can be modeled quantitatively on the basis of a sequential four-state mechanism with a well-populated early folding intermediate and a native-like late intermediate that manifests itself in unfolding experiments. Attempts to quantitatively model the folding kinetics of cytochrome *c* began as early as 1973 (Ikai et al., 1973), although there have been few studies since (Hagerman, 1977; Pryse et al., 1992). Recently there has been a resurgence of quantitative kinetic modeling studies on a variety of proteins (Kiefhaber et al., 1992; Jasanoff et al., 1994; Shastry et al., 1994; Houry et al., 1995; Kiefhaber, 1995; Parker et al., 1995, 1996; Shastry & Udgaonkar, 1995; Khorasanizadeh et al., 1996). As in our previous work on ubiquitin (Khorasanizadeh et al., 1996), we consider not only rates but also amplitudes and equilibrium values *versus* denaturant concentration in order to obtain a fully self-consistent kinetic description of folding and unfolding.

[1] Abbreviations: cyt c_2, *Rhodobacter capsulatus* ferricytochrome c_2; cyt *c*, horse cytochrome *c*; GuHCl, guanidine hydrochloride; V-plot, plot of the logarithm of folding and unfolding rates *vs* denaturant concentration.

MATERIALS AND METHODS

Materials. Rhodobacter capsulatus cyt c_2 was prepared by introducing the cytochrome c_2 gene into *Rb. capsulatus* cyt c_2 minus strain, as described elsewhere (Gooley et al., 1990; Caffrey et al., 1992). GuHCl was ultrapure grade from ICN-Schwarz/Mann. All other chemicals were reagent grade. GuHCl concentration was determined by refractive index measurement (Pace, 1986) on a Reichert-Jung Mark II Abbe refractometer (Leica, Inc., New York).

Equilibrium Fluorescence Measurements. Equilibrium fluorescence measurements were performed on an SLM Aminco-Bowman luminescence spectrometer. Native and unfolded solutions of cyt c_2 were prepared by passing the protein, oxidized with $K_3Fe(CN)_6$, through a column of Sephadex G-25 which had been preequilibrated at pH 5 with the folding buffer (25 mM phosphate and 25 mM acetate) or the unfolding buffer (6 M GuHCl in 25 mM phosphate and 25 mM acetate), respectively. Both solutions had a protein concentration of ~10 μM, as determined by UV absorption. For each measurement, an aliquot from the unfolded protein solution was removed from the cuvette to measure GuHCl concentration, and an equal volume from the native protein solution was added. Each fluorescence measurement was an average of 30 points collected during a 1-min time trace following 15−20 min of equilibration. The fluorescence of *N*-acetyltryptophan, prepared at the same concentration (~10 μM), was used to normalize the protein fluorescence. All measurements were made at 10 °C. The excitation wavelength was 280 nm, and the emission was observed at 350 nm. GuHCl denaturation curves were measured in the presence and absence of 0.4 M Na_2SO_4. Equilibrium data were fit by nonlinear least-squares analysis using the standard two-state model (Tanford, 1970), based on the linear free energy relationship:

$$\Delta G_U = \Delta G_0 - mC = m(C_m - C) \quad (1)$$

where ΔG_U is the free energy of unfolding, ΔG_0 is the unfolding free energy in the absence of denaturant, C is the denaturant concentration, C_m is the midpoint denaturant concentration where $\Delta G_U = 0$, and m is the slope of the transition. The fluorescence of the native and unfolded states was assumed to depend linearly on denaturant concentration, and the corresponding slopes and intercepts were used as fitting parameters in addition to C_m and m.

Optically-Detected Stopped-Flow Measurements. All fluorescence-detected kinetic folding experiments were performed on a PQ/SF-53 stopped-flow instrument (Hi-Tech, Salisbury, England) with a Berger-type mixer and a 2 × 2 × 10 mm^3 flow cell. A 75-W xenon lamp (On-Line Instrument Systems, Inc., Jefferson, GA) and a monochromator (Hi-Tech) were used to excite at 280 nm along the 10-mm axis of the flow cell. The fluorescence emission was measured in the 2-mm direction through a 320-nm cut-on glass filter. All stopped-flow experiments were performed at 10.0 °C. The initial GuHCl concentration in *re*folding experiments was 3.2 M in the absence of sodium sulfate and 4.6 M in the presence of 0.4 M Na_2SO_4. Final GuHCl concentrations (in refolding) after mixing were 0.55−2.1 M and 0.8−3.0 M in the absence and presence of 0.4 M Na_2SO_4, respectively. The initial GuHCl concentration in *un*folding experiments was 1.2 M and 2.0 M in the absence and presence of Na_2SO_4, respectively. Final GuHCl concentrations during unfolding were 2.0−5.7 M and 2.8−5.7 M in the absence and presence of Na_2SO_4, respectively. The initial concentration of cyt c_2 in all experiments was ~145 μM. The dead-time of the Hi-Tech apparatus was determined to be 2.2 ± 0.2 ms by monitoring the fluorescence reaction of 8-hydroxyquinoline with Mg^{2+} (Brissette et al., 1989).

Imidazole binding experiments were monitored by absorbance with a Biologic SFM4 stopped-flow instrument (Biologic, 38640 Claix, France) with a 2-mm flow cell. A tungsten lamp (LS-10, Hi-Tech) and monochromator were used to monitor the Soret region (418 nm) of cyt c_2. The charge transfer band at 699 nm, indicative of native Met96−Fe^{3+}−His17 ligation, disappears in the presence of high imidazole concentrations (>20 mM), and the Soret band (411 nm) is blue-shifted. All solutions were at pH 7.5 to ensure that the imidazole was deprotonated and could bind the heme iron. The kinetics of deligation and imidazole binding were monitored at various GuHCl concentrations by rapidly mixing native cyt c_2 with imidazole, yielding a final imidazole concentration of 0.25 M and final GuHCl concentrations of 0−1.5 M.

Kinetic data were collected and analyzed using software written in the ASYST programming language (Keithley Metrobyte). Data were acquired at a continuous sampling rate of 49 μs for 10−600 s and logarithmically averaged during acquisition to yield 90−115 data points, representing between 9 × 10^4 and 2.6 × 10^6 actual acquired points. Multiple traces were averaged to further improve signal-to-noise. Analysis was performed by nonlinear least-squares fitting of multiple exponential phases, except in the case of unfolding and imidazole binding experiments where only one exponential phase was observed. No weighting function was used during fitting.

Kinetic Modeling. To calculate the microscopic rate constants, k_j, defined in Scheme 1, a rate matrix was defined based on the set of linear differential equations describing the model (Scheme 1). Eigenvalues were calculated by reducing the rate matrix to the Hessenberg form, and then transforming the Hessenberg matrix into an upper triangular matrix, using a program written in the ASYST language [cf. Khorasanizadeh et al. (1996)]. The eigenvalues, λ_i (i = 1−3), correspond to the macroscopic rate constants (observable rates). The microscopic rate constants, k_j, are defined by two values, k°_j (k_j in the absence of GuHCl) and $m^\ddagger_j$ (GuHCl-dependence of k_j) according to the equation:

$$\ln k_j = \ln k^\circ_j + m^\ddagger_j C/RT \quad (2)$$

which is analogous to the linear relationship between ΔG and the denaturant concentration, C. The amplitudes associated with each eigenvalue were calculated from the eigenvectors and the observable signal for each state. The calculation also yields equilibrium values, which can be compared with the experimentally determined GuHCl denaturation curve. In order to compare the experimentally-determined fast phase amplitudes, A_1, with the predicted amplitudes, A_1 was normalized by dividing it by the factor $f_U - (f_N + A_2 + A_3)$, where f_U is the unfolded base line extrapolated to C, f_N is the native base line value at C, A_2 is the amplitude of the intermediate phase (0−10%), and A_3 is the amplitude of the slow phase (0−30%).

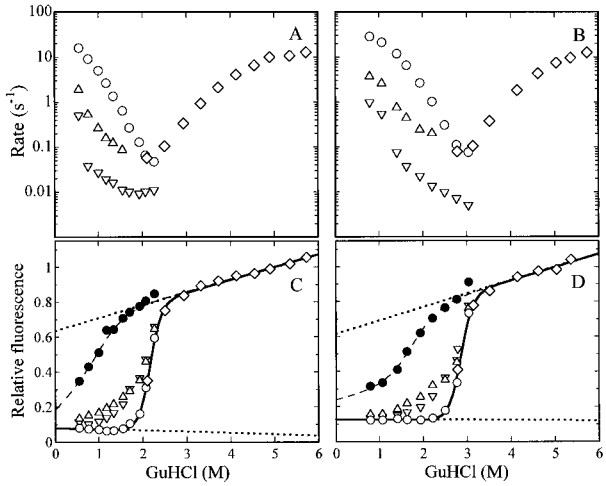

FIGURE 2: Denaturant-dependence of the folding and unfolding kinetics of oxidized cyt c_2 at pH 5, 10 °C, in the absence (A, C) and presence (B, D) of 0.4 M Na_2SO_4. In panels A and B, the observed folding/unfolding rates are plotted on a logarithmic scale as a function of GuHCl concentration. The kinetics of unfolding (◇) are monophasic. The kinetics of refolding were fit to three exponential phases: a major fast phase (○), a minor intermediate phase (△) with a 10-fold slower rate, and a minor slow phase (▽). As a representative example, the fit to the kinetic trace at 0.77 M GuHCl yielded the following apparent rates, amplitudes, and standard deviations: $k_1 = 8.9 \pm 0.1$ s^{-1}, $A_1 = 0.26 \pm 0.01$; $k_2 = 0.55 \pm 0.03$ s^{-1}, $A_2 = 0.060 \pm 0.001$; $k_3 = 0.033 \pm 0.008$ s^{-1}, $A_3 = 0.019 \pm 0.001$. In panels C, D, filled circles represent the initial fluorescence amplitude (extrapolated to zero time). The cumulative amplitudes of the two slower phases (△) were used to normalize the amplitude of the major phase in Figure 3 (see Materials Methods). The base line fluorescence at long folding/unfolding times (○, ◇) represents the equilibrium fluorescence as a function of GuHCl concentration, fitted to a two-state unfolding transition (solid line; see Table 1). The amplitude of the fast process (●) has also been fitted to a two-state transition (dashed curve). The dotted lines are linear extrapolations of the folded and unfolded base lines.

RESULTS

Equilibrium Denaturation. The GuHCl-induced unfolding transition of cyt c_2 was monitored by tryptophan fluorescence at 10 °C and pH 5, in the absence and presence of sodium sulfate (data not shown). Cyt c_2 has a single tryptophan residue at position 67, in close proximity to the heme, with low (5%) solvent-accessible surface area (identical to Trp59 of horse cyt *c*). Fluorescence is greatest in the unfolded state and almost entirely quenched in the native state due to energy transfer from the tryptophan to the heme (cf. Figure 2, solid line). The transition midpoint, C_m, and the slope, *m*, calculated by least-squares analysis of eq 1, are shown in Table 1. The C_m increases from 2.14 M ($\Delta G_0 = 8.58$ kcal mol^{-1}) to 2.75 M GuHCl ($\Delta G_0 = 10.45$ kcal mol^{-1}) upon addition of Na_2SO_4, corresponding to a $\Delta\Delta G_0$ of 1.9 kcal mol^{-1} (Table 1). For comparison, under the same conditions (10 °C, pH 5) in the absence of Na_2SO_4, horse cytochrome *c* has a C_m of 2.59 M GuHCl and an *m*-value of 3.9 kcal mol^{-1} M^{-1} with a corresponding ΔG_0 of 10.1 kcal mol^{-1} (Elöve et al., 1994). These equilibrium data are consistent with hydrogen exchange measurements on the two cytochromes, which showed substantially lower protection factors for *Rb. capsulatus* cyt c_2 (Gooley et al., 1990) compared to horse cyt *c* (Wand et al., 1986; Jeng et al., 1990), especially in the N-terminal helix.

Effect of GuHCl on Folding and Unfolding Kinetics. The stopped-flow method was used to monitor the fluorescence of Trp67 during folding and unfolding of cyt c_2 at various final GuHCl concentrations. At low GuHCl concentrations (below $C_m - 0.5$), three kinetic phases are observed (Figure 2A,B). In addition to the observed kinetics, there is an unresolved rapid drop in fluorescence (burst phase) within the dead-time of the instrument that accounts for as much as ~65% of the total amplitude in folding (solid circles in Figure 2C,D). At GuHCl concentrations of $C_m \pm 1.5$ M, the logarithm of the rate of the fastest observable process shows a V-shaped behavior with approximately linear increase above and below C_m, as expected for a two-state folding/unfolding transition. However, at both high (>4 M) and low (<1 M) GuHCl concentrations, the denaturant-dependence of the observed rates begins to level off. The nearly denaturant-independent plateau in the refolding rates is most pronounced in the presence of 0.4 M Na_2SO_4 where the V-plot is shifted to higher GuHCl concentrations (Figure 2B). In the transition region, the apparent rate of refolding decreases and reaches a minimum at C_m, over 2 orders of magnitude slower than the rate at the lowest GuHCl concentration measured. Within the transition region, the intermediate phase merges into the fast phase, and only the fast and slow phases are observed. In unfolding experiments ending at GuHCl concentrations above C_m, only one kinetic phase is observed with no evidence for any "missing" amplitude. Initially, the rate of unfolding increases steeply with increasing denaturant concentration, but at higher GuHCl concentrations (>4 M), the rate becomes nearly GuHCl-independent and reaches a limiting value of approximately 10 s^{-1}.

The observation of nonlinear rate profiles with decreasing slopes at low and high GuHCl concentrations (Figure 2A,B) and missing amplitude in refolding (Figure 2C,D) is inconsistent with a simple two-state process (Ikeguchi et al., 1986; Matouschek et al., 1990; Khorasanizadeh et al., 1996). The complex denaturant dependence of the observed rates is most easily explained by the presence of intermediates under both refolding and unfolding conditions. This was confirmed by quantitative modeling which showed that at least four states are required to fit the observable data. Additional states would be required to account for the intermediate and slow phases, which represent only a fraction of the total amplitude; the intermediate and slow phases cumulatively never account for more than 35% of the total observed amplitude (triangles in Figure 2C,D). The origin of the middle phase is unclear, although there is some evidence that it is due to a minor species (<10% of the total amplitude) with a non-native heme ligand [cf. Elöve et al. (1994)]. The slowest phase is consistent with a minor species refolding along a parallel pathway in which proline *cis/trans* isomerization is rate-limiting. The shallow denaturant-dependence of this rate (Figure 2A) suggests that peptide bond isomerization is only weakly coupled with the conformational events on the main folding pathway. To simplify the analysis, we have neglected these minor parallel folding events in our kinetic model.

Deligation of Met96 during Unfolding. Imidazole is known to bind the oxidized heme iron of cytochromes *c* under native conditions (Saleem & Wilson, 1988a), which displaces the native Met ligand and results in a native-like complex, M^{Im} (Shao et al., 1995). In order to understand the contribution of the methionine−iron linkage in unfolding, we measured the kinetics of binding imidazole to native cyt

Table 1: Effect of Na_2SO_4 on Cyt c_2 Stability Measured by GuHCl Denaturation[a]

method	$[Na_2SO_4]$ (M)	C_m (M)	m (kcal mol^{-1} M^{-1})	ΔG (kcal mol^{-1})	$\Delta\Delta G_{sulfate}$ (kcal mol^{-1})
equilibrium	0.0	2.14 ± 0.01	4.01 ± 0.16	8.58 ± 0.34	
	0.4	2.75 ± 0.01	3.80 ± 0.33	10.45 ± 0.91	1.87 ± 0.97
stopped-flow[b]	0.0	2.15 ± 0.01	4.32 ± 0.24	9.29 ± 0.52	
	0.4	2.85 ± 0.02	4.12 ± 0.50	11.74 ± 1.4	2.45 ± 1.5
kinetic model[c]	0.0	2.15	4.15	8.93	
	0.4	2.84	4.15	11.79	2.86

[a] All measurements were performed at 10 °C and pH 5. [b] Fluorescence-detected stopped-flow base lines after 10−600 s of refolding/unfolding. All errors are one standard deviation. [c] $\Delta G = (\Delta G_{NM} + \Delta G_{MI} + \Delta G_{IU})$, $m = m^{\ddagger}_{NM} + m^{\ddagger}_{MI} + m^{\ddagger}_{IU} - (m^{\ddagger}_{UI} + m^{\ddagger}_{IM} + m^{\ddagger}_{MN})$ and $C_m = \Delta G/m$; the kinetic parameters are listed in Table 2.

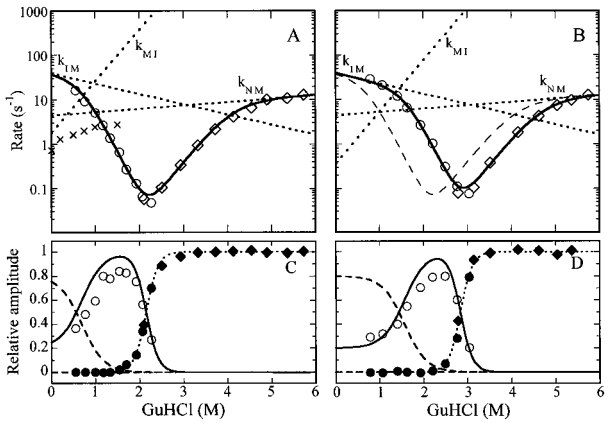

FIGURE 3: Kinetics of folding and unfolding of oxidized cyt c_2 at pH 5, 10 °C, in the absence (A, C) and presence (B, D) of 0.4 M Na_2SO_4. Panels A and B show the folding/unfolding rates of the major phase from Figure 2 as a function of GuHCl concentration. Panels C and D show the normalized amplitudes of the major folding phase (Y) and the normalized base line values from refolding (●) and unfolding (◆) experiments. The solid lines represent the rates (upper panels) and amplitudes (lower panels) predicted by solving the rate equations corresponding to the four-state model (Scheme 1). Only the rates corresponding to the lowest eigenvalue, λ_1, are shown (the two faster eigenvalues are off-scale). To emphasize the effect of Na_2SO_4 on the rates, the rate profile in the absence of Na_2SO_4 from panel A is reproduced in panel B (long dashes). The dotted lines show the microscopic rate constants (k_j, eq 2, Table 2) used to fit the data. The curvature in the rate plot at low [GuHCl] indicates the rate-limiting I→M transition, and the curvature at high [GuHCl] denotes the rate-limiting N→M deligation process. In panel A, the observed rate of deligation of Met96 (×), measured by imidazole binding kinetics, is shown for comparison with the rate constant k_{NM}. The dashed lines in the lower panels represent the predicted amplitude of a faster folding process with a rate >1000 s^{-1} (burst phase). The dotted line in the lower panels indicates the predicted unfolding equilibrium transition.

c_2. Imidazole binding results in disappearance of the 699 nm band in cyt c_2, signifying the loss of the native Met96−Fe^{3+}−His17 ligation. A blue-shift in the Soret band was also observed upon binding, and this wavelength (418 nm) was monitored during kinetic imidazole-jump experiments (Saleem & Wilson, 1988b). A control experiment at various final imidazole concentrations, in the absence of GuHCl, showed that the observed rate becomes imidazole-independent above 0.2 M imidazole (data not shown), indicating that the reaction is limited by breakage of the Met96−iron bond and any concomitant conformational changes rather than the second-order binding step. Stopped-flow experiments in which native cyt c_2 was exposed to 0.25 M imidazole show that the observed rate (× in Figure 3A) is approximately 1 s^{-1} in the absence of GuHCl and begins to approach the extrapolated rate constant k_{NM} at higher GuHCl concentrations.

Scheme 1

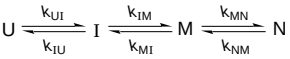

Quantitative Kinetic Modeling. Our laboratory has implemented a general matrix approach (Berberan-Santos & Martinho, 1990; Pogliani & Terenzi, 1992) to evaluate kinetic rate constants and amplitudes, which allows rapid analysis of different kinetic schemes. Figure 3 shows the denaturant-dependence of the observed rate for the main folding/unfolding phase and its relative amplitude, in the absence (left) and presence (right) of sodium sulfate. Amplitudes of the main observable process (lower panels) were normalized with respect to the total expected fluorescence change (see dotted lines in Figure 2) minus the contribution from the two slow phases. The curves were calculated by numerical analysis (see Materials and Methods), based on the four-state Scheme 1. In Scheme 1, U represents the unfolded state, I represents an ensemble of partially folded intermediates with largely quenched Trp67 fluorescence, M is a more native-like state, and N is the native state with the Met96/His17 pair of axial ligands. The fluorescence of Trp67 is assumed to be fully quenched in M and N due to efficient Trp−heme energy transfer. We will show below that the main distinction between M and N is the lack of the native Met96−iron bond in M. Because of the covalent bond between Cys16 and the heme, His17 remains bound to the iron in all four states. Since cyt c_2 has no additional histidines and all other potential ligands (amino terminus, lysines, etc.) are protonated at pH 5, U, I, and M are unlikely to contain a sixth ligand other than weakly bound solvent molecules. The denaturant-dependence of the microscopic rate constants is defined in eq 2. The intercepts k°_j and slopes $m^{\ddagger}_j$ of the six rate constants were varied manually, and the predicted rates and amplitudes were compared with the data in an effort to simultaneously fit the observed folding/unfolding rates, amplitudes, and equilibrium values at all denaturant and sulfate concentrations. Global least-squares analysis is not suitable for this type of modeling; some parameters are overdetermined at certain GuHCl concentrations, resulting in numeric instability. Systematic manual variation of the rate constants allows one to probe the effect of each parameter and achieve a consistent and well-determined fit. The relative fluorescence yields used for the different states were 1.0 for U, 0.2 for I, and 0 for M and N. The final kinetic parameters obtained are listed in Table 2.

It is not possible to determine unique values for all the kinetic parameters, since only the rate of the slowest phase, λ_1, can be measured; λ_2 and λ_3 occur within the dead-time of the stopped-flow apparatus. Thus, the U⇌I process is treated as a fast preequilibrium; since k_{UI} and k_{IU} are not

Table 2: Parameters for Kinetic Modeling[a]

$[Na_2SO_4]$(M)	K°_{UI}	$m^\ddagger_{IU}$[c]	k°_{IM}	$m^\ddagger_{IM}$[c]	k°_{MI}[d]	$m^\ddagger_{MI}$[b]	k°_{MN}[c,d]	k°_{NM}[c]
0.0	16	2.25	40	−0.3	1.8	1.5	10^5	4.5
0.4	530	2.25	40	−0.3	0.37	1.5	10^5	4.5

[a] The relative fluorescence of U is 1, I is 0.2, and M and N are 0. [b] Kinetic $m^\ddagger_j$-value (eq 2) in units of kcal mol^{-1} M^{-1}. [c] $m^\ddagger_{MN} = 0$ and $m^\ddagger_{NM} = 0.1$. [d] Only the ratio k_{MI}/k_{MN} is experimentally determined; k_{MN} is simply shown for clarity.

directly observable, only the preequilibrium constant K_{UI} can be measured (where $K_{UI} = k_{UI}/k_{IU}$). Although the general solution of a four-state kinetic mechanism is complex and was obtained numerically, $\lambda_1 = k_f + k_u$ can be approximated by the following expressions:

$$k_f = \frac{k_{UI}}{k_{UI} + k_{IU}} k_{IM} \quad (3)$$

$$k_u = \frac{k_{MI}}{k_{MI} + k_{MN}} k_{NM} \quad (4)$$

where k_f is the observed folding rate and k_u is the observed unfolding rate. At low GuHCl concentration (<0.5 M GuHCl), the U⇌I equilibrium lies toward I ($k_{UI} \gg k_{IU}$), and the observed folding rate (eq 3) simplifies to $k_f = k_{IM}$. At ~0.75 M GuHCl (in the absence of Na_2SO_4), $k_{UI} \sim k_{IU}$, and the observed rate is described by eq 3. At higher denaturant concentration (1−2 M GuHCl), the preequilibrium favors the unfolded state ($k_{UI} \ll k_{IU}$), and the observed rate, λ_1, is given by $K_{UI}k_{IM}$. Near C_m, the intermediate is highly destabilized, and its population is negligible ($K_{UI} \ll 1$).

In refolding experiments at low denaturant concentration, the formation of the native-like state M from I is rate-limiting and λ_1 approaches k_{IM}. The population of I is proportional to the "missing amplitude", $A_0 = 1 - A_1$, where A_1 is the normalized amplitude of the main observable phase, λ_1 (after subtraction of the minor slow phases). As the GuHCl concentration increases (below C_m), the intermediate is progressively destabilized, shifting the U⇌I equilibrium toward U; the observable phase gains amplitude, and its rate decreases sharply. In the region below C_m where the decrease in log(λ_1) becomes linear, the kinetics approaches apparent two-state behavior. However, since $\lambda_1 = K_{UI}k_{IM}$, the residual population of I still affects the rate and dominates its denaturant dependence [cf. Khorasanizadeh et al. (1996)].

According to our kinetic model (Scheme 1), the curvature in the rate profile at high GuHCl concentration is due to a change in the rate-limiting step in unfolding. Below about 4 M GuHCl, the main structural transition, M→I, with its strongly denaturant-dependent rate k_{MI} dominates the rate of unfolding, while above 5 M, the N→M transition with the nearly GuHCl-independent rate k_{NM} becomes rate-limiting. As in our previous studies on horse cytochrome *c* (Elöve et al., 1994; Colón et al., 1996), we attribute this step to the deligation of the Met 96−heme ligand. In this limit, k_{MI} is much larger than k_{MN}, and, according to eq 4, the observed unfolding rate, λ_1, approaches k_{NM}. Near 4 M GuHCl, $k_{MI} \sim k_{MN}$ and λ_1 is described by eq 4. Because of the steep denaturant dependence of k_{MI} (Figure 3A,B), methionine ligation (M→N) is faster than unfolding of M ($k_{MN} \gg k_{MI}$) at lower denaturant concentration, in the steep part of the rate profile above C_m. In this limit, eq 4 simplifies to $\lambda_1 = (k_{MI}/k_{MN})k_{NM}$, where $(k_{MI}/k_{MN}) \ll 1$, so that the observed unfolding rate is much slower than the rate of deligation. The equation can also be written as $\lambda_1 = K_{NM}k_{MI}$, where the denaturant-independent ligation/deligation terms are grouped together and $K_{NM} \ll 1$ at all denaturant concentrations.

The effect of Na_2SO_4 on the folding/unfolding kinetics of cyt c_2 can be modeled by changing only two kinetic parameters, K_{UI} and k_{MI}; none of the GuHCl dependencies ($m^\ddagger_j$ values) of the microscopic rate constants were modified (see Table 2). By increasing K_{UI} by a factor of 33 and decreasing k_{MI} by a factor of 5, we were able to accurately model the observed denaturant-dependence of rates and amplitudes, as well as the equilibrium data (Figure 3, panels B and D).

The four-state model quantitatively reproduces the observed rates of folding and unfolding at all denaturant concentrations, both in the presence and in the absence of sodium sulfate (Figure 3, panels A and B). The predicted equilibrium transitions (dotted curves in panels C and D) are also in excellent agreement with the observed equilibrium values (solid symbols) measured at the end of each kinetic trace. The corresponding C_m and *m* values are listed in Table 1 for comparison with the parameters calculated from the equilibrium denaturation curves (data not shown). However, the amplitude of the major phase predicted by the model does not exactly fit the experimental amplitude. Possible explanations include additional intermediate(s) not included in the model and/or errors caused by neglecting the minor slow phases.

Alternate Models. Several alternate four-state mechanisms were also examined. In the first case, I is a dead-end intermediate that must completely unfold before productive folding can continue (I⇌U⇌M⇌N). Although it is impossible to conclusively prove by formal kinetic analysis whether this model or Scheme 1 is correct, we feel that a sequential model provides a self-consistent description and leads to a physically more plausible description (Khorasanizadeh et al., 1996). A second possible mechanism is U⇌I⇌N with M formed in an off-pathway reaction from I. This is the minimal mechanism for a stable misfolded state. The prediction is that an increase in the apparent folding rate would be observed at low denaturant concentrations as the intermediate, M, becomes progressively destabilized by the increasing denaturant. However, this model cannot self-consistently predict both the folding *and* unfolding behavior that we observe at low and high GuHCl concentrations. A third possible mechanism is a circular pathway that corresponds to Scheme 1 if direct conversion between U and N were possible. If U→N were fast, it would result in apparent two-state kinetics. The U→N step affects the observed folding kinetics only if it is comparable to the rate-limiting step along the other pathway (I→M). For example, a direct path to N might diminish the lag in the accumulation of N predicted by Scheme 1 [cf. Kiefhaber (1995b)]. However, it would be difficult to measure this lag phase, since I accumulates during the dead-time. Moreover, a circular scheme requires four additional parameters. Although it is never possible to exclusively prove a particular kinetic mechanism, Scheme 1 is able to accurately model all of the available kinetic data.

Free Energy Diagrams. Free energy diagrams were calculated on the basis of the kinetic parameters in Table 2

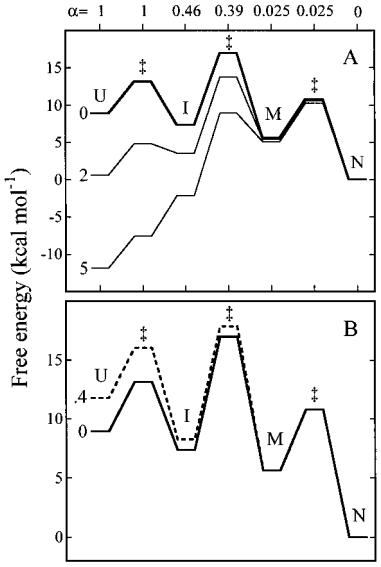

FIGURE 4: Free energy diagrams calculated on the basis of the kinetic parameters in Table 2. The barrier for the kinetically unresolved U⇌I transition was calculated based on the measured value for $K_{UI} = k_{UI}/k_{IU}$, assuming a GuHCl-independent rate constant of $k_{UI} = 5 \times 10^5$ s^{-1}. Panel A: The free energy, calculated according to eq 5, for the four states in Scheme 1 at three different GuHCl concentrations (0, 2, 5 M) in the absence of Na_2SO_4. Panel B: Effect of 0.4 M Na_2SO_4 on the free energies (dashed line). The native state is arbitrarily set to a free energy of zero. The numbers at the top refer to the increment in solvent-accessible surface area relative to the native state, N, defined as $\alpha_i = \Sigma m^{\ddagger}_i/m$, which can be considered as a reaction coordinate for unfolding.

(Figure 4). The activation energy required to cross the barrier between each state was calculated based on k°_j and $m^{\ddagger}_j$ (Table 2) according to the equation:

$$\Delta G^{\ddagger} = -RT\,(\ln k^{\circ}_j/A_o) - m^{\ddagger}_j C \qquad (5)$$

A_o is the Arrhenius preexponential factor (arbitrarily chosen as 10^9 M^{-1} s^{-1}). Using the native state in the absence of Na_2SO_4 as the reference, the free energy of the unfolded state, ΔG_{UN}, is predicted to be 8.9 kcal mol^{-1}, close to the experimental value of 9.3 ± 0.5 kcal mol^{-1} determined from the stopped-flow base line data (Table 1). In the presence of Na_2SO_4, ΔG_{UN} is predicted to be 11.8 kcal mol^{-1}, compared to the experimental value of 11.7 ± 1 kcal mol^{-1}.

DISCUSSION

Folding Mechanism. We have shown that the effect of GuHCl and Na_2SO_4 on the folding/unfolding kinetics of cytochrome c_2 can be quantitatively modeled with a minimal four-state mechanism (Scheme 1). Although it is difficult to formally exclude alternative models with off-pathway intermediates [cf. Khorasanizadeh (1996)], we feel that the sequential mechanism leads to physically plausible predictions. Our kinetic analysis indicates that the rate-limiting step in refolding is the formation of a native-like state, M, from a folding intermediate, I, which is in rapid (<2 ms) equilibrium with the unfolded state. Under stabilizing conditions (low GuHCl concentration, especially in the presence of Na_2SO_4), I is well-populated and gives rise to a pronounced missing amplitude effect (Figure 2C,D). The observation that with decreasing GuHCl concentration the initial fluorescence signal (extrapolated to zero time) approaches the native baseline value to within 20% indicates that I has a compact conformation with Trp67 in close proximity to the heme, which largely quenches its fluorescence. The GuHCl-dependence of the initial fluorescence signal seen in Figure 2C closely resembles that previously described for horse cytochrome *c* (Colón et al., 1996; Sosnick et al., 1996), indicating that both proteins exhibit compact early intermediates with similar stability. Previous kinetic CD studies on horse cytochrome *c* have shown that this intermediate contains native-like helical secondary structure (Elöve et al., 1992), which is likely to be the case for cyt c_2 as well. In the presence of sodium sulfate, the initial signal shows a pronounced sigmoidal denaturant dependence (Figure 2D), suggesting that I is a distinct thermodynamic state (ensemble of compact conformations) that undergoes a cooperative (two-state) unfolding transition.

At low GuHCl concentrations, the early intermediate I is fully populated, and the rate-limiting I→M transition can be directly measured. As I is destabilized by addition of denaturant, the observed rate (eq 3) slows down along with the decreasing population of I. The native-like intermediate M does not accumulate under refolding conditions, since k_{MN} is much larger than the rate-limiting k_{IM}. Thus, the refolding kinetics of cyt c_2 are well described by a three-state model analogous to that used in our recent work on ubiquitin (Khorasanizadeh et al., 1996), and many of the conclusions drawn there can be applied to cyt c_2. For example, in both cases the rate-limiting step depends only weakly on denaturant concentration, suggesting that the main transition state resembles I in terms of solvent-accessible surface area. However, in comparison to wild-type ubiquitin, k_{IM} is ~10-fold smaller for cyt c_2 (Table 2), and the population of I is somewhat higher, especially in the presence of Na_2SO_4 (K_{UI} = 530, compared to 200 for ubiquitin under similar conditions). In the unfolding transition region, the population of I is negligible, and the folding kinetics appear two-state. In terms of the free energy diagrams in Figure 4A (middle trace at 2 M GuHCl), this means that both I and M are above U and N in free energy, so that U and N are the only states with significant population. However, in contrast to the conventional two-state description, our model predicts that formation of a collapsed intermediate remains an obligatory step in folding even in the transition region, so that the residual population of I continues to affect the observed rate according to the relationship $\lambda = K_{UI} \cdot k_{IM}$. Because of the weak denaturant dependence of k_{IM}, we attribute the steep decrease in the observed folding rate with increasing denaturant concentration (below C_m) primarily to the destabilization of I. In other words, the rate-limiting barrier between I and M tracks the increase in the energy level of I relative to U (Figure 4A). The consistency of our kinetic analysis is confirmed by the excellent agreement between the predicted and observed equilibrium transition (Figure 3C,D, Table 1).

Unfolding Mechanism of Cyt c_2. The sharp change in slope in the rate profile at high GuHCl concentrations provides clear evidence for the formation of an unfolding intermediate, M, which limits the rate of unfolding under strongly denaturing conditions, where the main structural unfolding step (M→I) is fast. The weak denaturant dependence of k_{NM} compared to the equilibrium *m*-value ($m^{\ddagger}_{NM}/m$ = 0.025; cf. Tables 1 and 2, Figure 3) shows that M is a native-like intermediate with only slightly larger solvent-accessible surface than N. In the case of horse cytochrome

c, which shows very similar unfolding behavior, we have previously attributed this effect to the dissociation of the axial methionine ligand (Colón et al., 1996). This interpretation is confirmed by recent kinetic measurements in the presence of imidazole, which displaces the native Met80 ligand in cyt *c* and gives rise to a linear V-plot up to high GuHCl concentrations without any indication of a rate-limiting unfolding step (Colón, Sauder, and Roder, in preparation). To test this hypothesis in the case of cyt c_2, we monitored the deligation kinetics of Met96 ($N \rightarrow M^{Im}$), treating the imidazole-bound form of cyt c_2 as a structural analogue to state M in our model. The observed rate ($\times$ in Figure 3A) is ~4-fold slower than the rate constant k_{NM} extrapolated to low GuHCl concentrations, but approaches k_{NM} to within a factor 2. This discrepancy is not surprising, considering the long extrapolation of the rate constant from >5 M GuHCl, and the fact that the unfolding kinetics were measured at pH 5.0, whereas ligand binding was measured at pH 7.5. Thus, both the rate of ligand binding under native conditions and the rate of unfolding at high GuHCl concentrations appear to reflect a common rate-determining step, namely, the dissociation of the axial methionine ligand.

At first sight, the curvature in the rate profiles at both extremes of denaturant concentration suggests that the kinetic role of the intermediate M in unfolding is analogous to that of I in refolding. However, inspection of the free energy diagram in Figure 4A shows that the mechanisms of unfolding and refolding are quite different. While the folding intermediate I is well-populated under stable refolding conditions (it occurs before the largest barrier and has lower free energy than U), the unfolding intermediate M is not well-populated, since its energy is higher than that of the initial state, N, under all conditions. It can be detected only because of the change in rate-limiting steps from the M→I transition at intermediate GuHCl concentration to the N→M transition at high GuHCl concentration. In contrast, the barrier between I and M remains the highest point of the free energy profile under all refolding conditions ([GuHCl] < C_m).

In spite of the complex denaturant dependence, unfolding occurs in a single exponential phase that accounts for the total expected fluorescence change under all conditions. The observation that the denaturant dependence of the unfolding rate levels off above ~5 M GuHCl without evidence of a second faster phase indicates that the methionine dissociation step (N→M) precedes the main structural unfolding step under all conditions investigated. Apparently, the native structure does not unfold readily without first breaking the Met96 sulfur−iron bond, which serves as a strongly stabilizing cross-link. This situation is clarified by Scheme 2, where we include a (hypothetical) Met96-ligated unfolded state (U^M) in addition to the four states of Scheme 1. In Scheme 2, the unfolding pathway through M is preferred as long as the deligation step (N→M) is faster than direct unfolding of the methionine-ligated protein ($N \rightarrow U^M$). This is the case up to the highest GuHCl concentration studied (5.8 M). The long-range Met96−heme cross-link apparently provides sufficient kinetic stability to the native state to render direct unfolding from N to U^M much slower than unfolding of the deligated species (see dotted line labeled k_{MI} in Figure 3). At intermediate denaturant concentrations, the observed unfolding process follows the steep denaturant-dependence of k_{MI}, but its rate is nearly 5 orders of magnitude slower because of the highly unfavorable ligand dissociation equilibrium constant, k_{NM}/k_{MN} (Table 2). The observed unfolding rate continues to increase up to ~5 M GuHCl, where it approaches k_{NM} and begins to level off. Scheme 2 predicts that the shallow denaturant dependence continues until the direct unfolding rate ($N \rightarrow U^M$) approaches k_{NM}, at which point we expect a renewed increase in the observed rate. The fact that this does not occur up to the highest GuHCl concentration measured (Figure 3A) indicates that the $N \rightarrow U^M$ rate is less than 10^{-6} s^{-1} at 0 M GuHCl (assuming $m^{\ddagger}_{NU^M} = m^{\ddagger}_{NM} + m^{\ddagger}_{MI} = 1.5$ kcal mol^{-1} M^{-1}).

Scheme 2

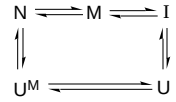

The dissociation of the Met96 sulfur from the heme iron during the N→M transition appears to be coupled with some localized structural rearrangements, as indicated by the small, but significant denaturant-dependent increase in the rate constant k_{NM}, as well as in the rate of imidazole binding at low denaturant concentration (Figure 3A). Thus, we expect k_{NM} to be correlated with the local structural stability in the vicinity of the methionine ligand. Comparison with previous unfolding studies on horse cytochrome *c* shows a striking qualitative similarity in the denaturant dependence, but significant variations are seen in the limiting unfolding rate at high denaturant concentration (all data at 10 °C): 12 s^{-1} for cyt c_2 at 5.8 M GuHCl (Figure 3A,B), compared to 50 s^{-1} for horse cytochrome *c* at pH 7 (Colón et al., 1996), ~80 s^{-1} at pH 5.0 (Colón et al., unpublished), and ~120 s^{-1} at pH 4.9 and higher salt concentration (Sosnick et al., 1996). By these criteria, the bacterial protein has a more stable ligand environment than the horse protein. Another parameter related to the stability of the methionine−iron interaction is the apparent p*K* of the alkaline transition, which is accompanied by replacement of the native methionine ligand with another side chain, such as a deprotonated lysine or tyrosine (Schechter & Saludjian, 1967; Davis et al., 1974; Bosshard, 1981; Gadsby et al., 1987; Nall et al., 1989). Cyt c_2 has a p*K* of 8.9 (Caffrey & Cusanovich, 1991b), while values in the range 9.1−9.3 have been reported for horse cytochrome *c* (Davis et al., 1974; Gadsby et al., 1987). The deligation-limited rate of unfolding is probably a more direct measure of local structural stability, since the alkaline transition also depends on the location of potential alternative ligands.

While the majority of proteins investigated show approximately linear plots of $\log(k_u)$ *vs* denaturant concentration above C_m, nonlinear unfolding behavior has been observed for a number of proteins other than cytochrome *c*, including carp parvalbumin (Lin & Brandts, 1978), α-lactalbumin (Ikeguchi et al., 1986), ribonuclease T2 (Kawata & Hamaguchi, 1995), TEM-1β-lactamase (Vanhove et al., 1995), and the arc-repressor dimer (Jonsson et al., 1996), although Jonsson et al. (1996) were the first to offer an interpretation. We recently observed a similar effect for *Staphylococcal* nuclease (Walkenhorst, Green, and Roder, in preparation). However, the examples with the most pronounced curvature in the rate profiles at high GuHCl are the *c*-type cytochromes (Ikai et al., 1973; Colón et al., 1996). Possible explanations include: (1) intrinsic nonlinearity in the effect of denaturant concentration on the free energy of transition states [Tanford,

1970; see also Parker et al. (1995)]; (2) a two-state model with a denaturant-induced shift in the transition state along the reaction coordinate (Matouschek & Fersht, 1993; Matouschek et al., 1994); and (3) a change in the rate-limiting barrier for unfolding as a function of denaturant concentration (Jonsson et al., 1996). The first explanation is not very plausible, since the curvature predicted by amino acid transfer free energies is insufficient to explain the sharp bend observed at high GuHCl concentrations. Furthermore, many equilibrium and kinetic studies [cf. Jackson et al. (1993), Khorasanizadeh et al. (1993), and Kragelund et al. (1995)] are fully consistent with a linear free energy model (Schellman, 1978; Agashe & Udgaonkar, 1995). The second explanation would also predict a more gradual curvature in the denaturant dependence of the observed rates, attributed to a gradual change in the solvent exposure of the transition state. The more abrupt change in slope of the log(k_u) *vs* [GuHCl] plot supports the third possibility, namely, that there are different rate-limiting barriers in unfolding at intermediate and high denaturant concentrations. In a recent study on two arc repressor variants, Jonsson et al. (1996) reached the same conclusion. They found that the rate of unfolding, coupled with dissociation of the native dimer, follows a linear plot of log(k_u) at low urea concentrations extending down to 0 M, but shows a pronounced downward curvature with increasing urea concentration above C_m. They concluded that this behavior is most readily explained with the third model, which is very similar to our interpretation of the cyt c_2 results. However, the structural origin of the early steps in unfolding is less apparent in the case of arc repressor.

Effect of Solvent Additives. Since GuHCl appears to destabilize folded proteins *via* preferential interaction with newly exposed surface regions in partially or fully unfolded states (Tanford, 1970; Schellman, 1978), we chose N as the reference state for comparing the free energy diagrams at different denaturant concentrations (Figure 4A). The divergence of the free energy profiles at three representative GuHCl concentrations shows that the solvent-accessible surface area of equilibrium and transition states increases continuously in going from N toward U. The numbers, α_i, in Figure 4 indicate the increase in surface area relative to N obtained by dividing appropriate sums of kinetic $m^{\ddagger}_j$-values (Table 2) by the equilibrium *m*-value (Table 1), which provides a measure of the progress of unfolding that can be used as a reaction coordinate [cf. Tanford (1970), Chen et al. (1992), and Jonsson (1996)]. As mentioned above, the small increase in area from N to M across the first barrier in unfolding is consistent with a tightly folded, native-like structure for M and the adjacent transition state. In the direction of refolding, the intermediate I has progressed just over halfway toward N in terms of this reaction coordinate ($m^{\ddagger}_{IU}/m = 0.54$), and the transition state between I and M is only slightly closer [$(m^{\ddagger}_{IU} + m^{\ddagger}_{IM}]/m = 0.61$].

The equilibrium *m*-values and the kinetic $m^{\ddagger}_j$-values are very similar in the presence and absence of 0.4 M Na_2SO_4 (Tables 1 and 2), indicating that the stabilizing salt does not interfere with the interaction of GuHCl with the protein. Thus, both agents act independently, and their effects are additive with opposite sign. The kinetic analysis (Table 2) shows that the effect of sodium sulfate can be modeled by adjusting only two parameters, K_{UI} and k_{MI}. A 33-fold increase in K_{UI} (stabilization of I relative to U) results in a corresponding increase in the rate of folding below the transition region, while a 5-fold decrease in k_{MI} lowers the observed unfolding rate above C_m. As a result, the V-shaped part of the log(rate) *vs* denaturant concentration plot shifts by about 0.65 M toward higher GuHCl concentrations (Figure 3), matching the corresponding change in C_m values (Table 1).

It is interesting that Na_2SO_4 affects only the strongly GuHCl-dependent unfolding transitions, I⇌U and M→I, while it has no effect on the weakly denaturant-dependent rate constants, k_{IM}, k_{MN}, and k_{NM} (Table 2). This seems reasonable, since the action of denaturing or stabilizing agents can be explained by favorable or unfavorable preferential interactions with partly or fully unfolded states (as opposed to specific binding to folded states). According to Timasheff (Timasheff & Arakawa, 1988; Timasheff, 1993), the stabilizing effect of salts, such as Na_2SO_4, on folded protein states can be understood in terms of their tendency to be excluded from the surface of the polypeptide chain, resulting in energetically unfavorable preferential hydration of surface groups. Thus, the salt disfavors any increase in solvent exposure and shifts the conformational equilibria toward more compact states. As illustrated by the free energy diagram in Figure 4B, addition of Na_2SO_4 destabilizes I to a smaller extent than U, relative to N ($\Delta\Delta G_{IN}/\Delta\Delta G_{UN} = 0.32$), as expected for a partially collapsed state with a solvent-accessible surface area intermediate between those of U and N. This conclusion is fully consistent with the GuHCl-dependence of the U⇌I transition and the fluorescence properties of I (~80% quenching of Trp67 fluorescence). The experimental finding that neither GuHCl nor Na_2SO_4 has a significant effect on k_{IM} indicates that the transition state in the rate-limiting conversion of I to M resembles the intermediate in terms of solvent exposure. Khorasanizadeh et al. (1996) recently reached the same conclusion, based on analogous observations on a series of ubiquitin mutants.

Folding in the Absence of Competing Axial Heme Ligands. The absence of potential non-native histidine or methionine ligands in *Rb. capsulatus* cyt c_2 results in a much simpler folding mechanism compared to other *c*-type cytochromes. Except for a very minor population of more slowly folding species (Figure 2), the fluorescence-detected folding kinetics are fully accounted for by a simple sequential mechanism (Scheme 1) with a well-populated burst-phase intermediate that dominates the kinetic behavior under stabilizing folding conditions. In contrast, a minimal folding mechanism for horse cytochrome *c* features at least one additional parallel pathway originating from unfolded species containing non-native histidine−iron bonds (Elöve et al., 1994; Colón et al., 1996). At near-neutral pH, the folding kinetics are dominated by intermediates on this pathway, including a burst intermediate, I_c^H, which is structurally analogous to I in Scheme 1, and a more highly structured state with interacting chain termini, I_{NC}^H (Roder et al., 1988; Elöve et al., 1994; Colón et al., 1996). Under stable refolding conditions at pH 5, folding occurs along a more direct pathway originating from an unfolded species without a strong sixth ligand (Elöve & Roder, 1991; Elöve et al., 1994; Sosnick et al., 1994). However, our recent analysis of the GuHCl-dependence of rates and amplitudes at pH 5.0 (Colón et al., in preparation) shows that kinetic complications due to non-native ligands make a major contribution under more destabilizing conditions. Some of these complications have

already been noted previously (Elöve et al., 1994; Figures 4 and 7), and are again apparent in the kinetic traces reported by Sosnick et al. (1996; Figure 1), but these workers chose a simplified two-state description in their analysis. Apparently, the mildly acidic, but nondenaturing conditions (pH ~5) cannot completely avoid the interference from non-native heme ligands.

On the other hand, cyt c_2, which has no additional histidines and methionines other than the native axial ligands, shows no evidence for ligand-dependent kinetic phases at pH 5, and its folding kinetics reveal the underlying structural events without interference from extraneous rate-limiting steps. This simplification also makes explicit kinetic modeling possible, which provides valuable information on the free energies of intermediates and kinetic barriers, and their dependence on solvent conditions (Figure 4). Thus, we were able to show that all experimental observations (rates, amplitudes, and equilibrium values *vs* GuHCl concentration in the presence and absence of Na_2SO_4) are fully consistent with a simple sequential mechanism featuring a prominent compact intermediate populated on the submillisecond time scale and a late folding intermediate (or early unfolding intermediate) lacking the Met96 sulfur−iron bond of the native structure. It is important to note that, contrary to previous conclusions (Sosnick et al., 1994, 1996), avoidance of non-native heme ligation produces apparent two-state folding/unfolding behavior only in the transition region, where both intermediates are unstable relative to the unfolded and native states (Figure 4).

The kinetic data for cyt c_2 show no direct evidence for a folding intermediate with interacting N- and C-terminal helices analogous to I_{NC} in horse cytochrome *c*. This is not surprising, since I_{NC} accumulates only under conditions where non-native histidine ligands form (pH >6), while its population is low at acidic pH where the alternate histidine ligands are protonated (Elöve et al., 1994). However, we have previously argued that docking of the N- and C-terminal helices is an early folding event even in the absence of non-native heme ligation (Elöve et al., 1994; Colón et al., 1996), which was confirmed by recent data on the effects of helix interface mutations on the kinetics of folding at acidic pH (Colón & Roder, 1996). Preliminary hydrogen exchange labeling results suggest that this may also be the case for cyt c_2 (Sauder, Zhao, MacKenzie, and Roder, in preparation).

ACKNOWLEDGMENT

We thank G. A. Elöve, W. Colón, S. Khorasanizadeh, and S. Luck for valuable advice and other members of the group for critical reading of the manuscript.

REFERENCES

Agashe, V. R., & Udgaonkar, J. B. (1995) *Biochemistry 34*, 3286−3299.
Ambler, R. P., Daniel, M., Hermoso, J., Meyer, T. E., Bartsch, R. G., & Kamen, M. D. (1979) *Nature 278*, 659−660.
Babul, J., & Stellwagen, E. (1972) *Biochemistry 11*, 1195−1200.
Benning, M. M., Wesenberg, G., Caffrey, M. S., Bartsch, R. G., Meyer, T. E., Cusanovich, M. A., Rayment, I., & Holden, H. M. (1991) *J. Mol. Biol. 220*, 673−685.
Berberan-Santos, M. N., & Martinho, J. M. G. (1990) *J. Chem. Educ. 67*, 375−379.
Bosshard, H. R. (1981) *J. Mol. Biol. 153*, 1125−1149.
Brems, D. N., & Stellwagen, E. (1983) *J. Biol. Chem. 258*, 3655−3660.
Brissette, P., Ballou, D. P., & Massey, V. (1989) *Anal. Biochem. 181*, 234−238.
Bushnell, G. W., Louie, G. V., & Brayer, G. D. (1990) *J. Mol. Biol. 214*, 585−595.
Caffrey, M. S., & Cusanovich, M. A. (1991a) *Arch. Biochem. Biophys. 285*, 227−230.
Caffrey, M. S., & Cusanovich, M. A. (1991b) *Biochemistry 30*, 9238−9241.
Caffrey, M. S., & Cusanovich, M. A. (1993) *Arch. Biochem. Biophys. 304*, 205−208.
Caffrey, M., Davidson, E., Cusanovich, M., & Daldal, F. (1992) *Arch. Biochem. Biophys. 292*, 419−426.
Chen, B.-L., Baase, W. A., Nicholson, H., & Schellman, J. A. (1992) *Biochemistry 31*, 1464−1476.
Chothia, C., & Lesk, A. M. (1985) *J. Mol. Biol. 182*, 151−158.
Colón, W., & Roder, H. (1996) *Nat. Struct. Biol.* (in press).
Colón, W., Elöve, G. A., Wakem, L. P., Sherman, F., & Roder, H. (1996) *Biochemistry 35*, 5538−5549.
Daldal, F., Cheng, S., Applebaum, J., Davidson, E., & Prince, R. C. (1986) *Proc. Natl. Acad. Sci. U.S.A. 83*, 2012−2016.
Davis, L., Schejter, A., & Hess, G. P. (1974) *J. Biol. Chem. 249*, 2624−2632.
Dyson, H. J., & Beattie, J. K. (1982) *J. Biol. Chem. 257*, 2267−2273.
Elöve, G. A., & Roder, H. (1991) *ACS Symp. Ser. 470*, 50−63.
Elöve, G. A., Chaffotte, A. F., Roder, H., & Goldberg, M. E. (1992) *Biochemistry 31*, 6876−6883.
Elöve, G. A., Bhuyan, A. K., & Roder, H. (1994) *Biochemistry 33*, 6925−6935.
Gadsby, M. A., Peterson, J., Foote, N., Greenwood, C., & Thomson, A. J. (1987) *Biochem. J. 246*, 43−54.
Gooley, P. R., & MacKenzie, N. E. (1990) *FEBS Lett. 260*, 225−228.
Gooley, P. R., Caffrey, M. S., Cusanovich, M. A., & MacKenzie, N. E. (1990) *Biochemistry 29*, 2278−2290.
Gooley, P. R., Caffrey, M. S., Cusanovich, M. A., & MacKenzie, N. E. (1991a) *Eur. J. Biochem. 196*, 653−661.
Gooley, P. R., Zhao, D., & MacKenzie, N. E. (1991b) *J. Biomol. NMR 1*, 145−154.
Gooley, P. R., Caffrey, M. S., Cusanovich, M. A., & MacKenzie, N. E. (1992) *Biochemistry 31*, 443−450.
Hagerman, P. J. (1977) *Biopolymers 16*, 731−747.
Houry, W. A., Rothwarf, D. M., & Scheraga, H. A. (1995) *Nat. Struct. Biol. 2*, 495−503.
Ikai, A., Fish, W. W., & Tanford, C. (1973) *J. Mol. Biol. 73*, 165−184.
Ikeguchi, M., Kuwajima, K., Mitani, M., & Sugai, S. (1986) *Biochemistry 25*, 6965−6972.
Jackson, S. E., elMasry, N., & Fersht, A. R. (1993) *Biochemistry 32*, 11270−11278.
Jasanoff, A., Davis, B., & Fersht, A. R. (1994) *Biochemistry 33*, 6350−6355.
Jeng, M.-F., Englander, S. W., Elöve, G. A., Wand, A. J., & Roder, H. (1990) *Biochemistry 29*, 10433−10437.
Jonsson, T., Waldburger, C. D., & Sauer, R. T. (1996) *Biochemistry 35*, 4795−4802.
Kawata, Y., & Hamaguchi, K. (1995) *Protein Sci. 4*, 416−420.
Khorasanizadeh, S., Peters, I. D., Butt, T. R., & Roder, H. (1993) *Biochemistry 32*, 7054−7063.
Khorasanizadeh, S., Peters, I. D., & Roder, H. (1996) *Nat. Struct. Biol. 3*, 193−205.
Kiefhaber, T. (1995a) in *Methods in Molecular Biology: Protein Stability and Folding: Theory and Practice* (Shirley, B. A., Ed.) pp 313−343, Humana Press, Totowa, NJ.
Kiefhaber, T. (1995b) *Proc. Natl. Acad. Sci. U.S.A. 92*, 9029−9033.
Kiefhaber, T., Kohler, H., & Schmid, F. X. (1992) *J. Mol. Biol. 224*, 217−229.
Kragelund, B. B., Robinson, C. V., Knudsen, J., Dobson, C. M., & Poulsen, F. M. (1995) *Biochemistry 34*, 7217−7224.
Kraulis, P. J. (1991) *J. Appl. Crystallogr. 24*, 946−950.
Lin, L.-N., & Brandts, J. F. (1978) *Biochemistry 17*, 4102−4110.
Mathews, F. S. (1985) *Prog. Biophys. Mol. Biol. 45*, 1−56.
Matouschek, A., & Fersht, A. R. (1993) *Proc. Natl. Acad. Sci. U.S.A.* 90, 7814−7818.

Matouschek, A., Kellis, J. T., Jr., Serrano, L., Bycroft, M., & Fersht, A. R. (1990) *Nature* 346, 440−445.
Matouschek, A., Matthews, J. M., Johnson, C. M., & Fersht, A. R. (1994) *Protein Eng. 7*, 1089−1095.
Meyer, T. E., & Kamen, M. D. (1982) *Adv. Protein Chem. 35*, 105−212.
Moore, G. R., & Pettigrew, G. W. (1990) *Cytochrome c: Evolutionary, Structural and Physiochemical Aspects*, Springer-Verlag, Berlin.
Nall, B. T., & Landers, T. A. (1981) *Biochemistry 20*, 5403−5411.
Nall, B. T., Zuniga, E. H., White, T. E., Wood, L. C., & Ramdas, L. (1989) *Biochemistry 28*, 9834−9839.
Pace, C. N. (1986) *Methods Enzymol. 131*, 266−280.
Parker, M. J., Spencer, J., & Clarke, A. R. (1995) *J. Mol. Biol. 253*, 771−786.
Parker, M. J., Sessions, R. B., Badcoe, I. G., & Clarke, A. R. (1996) *Folding Des. 1*, 145−156.
Pogliani, L., & Terenzi, M. (1992) *J. Chem. Educ. 69*, 278−280.
Pryse, K. M., Bruckman, T. G., Maxfield, B. W., & Elson, E. L. (1992) *Biochemistry 31*, 5127−5136.
Ridge, J. A., Baldwin, R. L., & Labhardt, A. M. (1981) *Biochemistry 20*, 1622−1630.
Roder, H., & Elöve, G. A. (1994) in *Mechanisms of Protein Folding: Frontiers in Molecular Biology* (Pain, R. H., Ed.) pp 26−55, Oxford University Press, New York.
Roder, H., Elöve, G. A., & Englander, S. W. (1988) *Nature 335*, 700−704.
Saleem, M. M. M., & Wilson, M. T. (1988a) *Inorg. Chim. Acta 153*, 93−98.
Saleem, M. M. M., & Wilson, M. T. (1988b) *Inorg. Chim. Acta 153*, 99−104.
Salemme, F. R. (1977) *Annu. Rev. Biochem. 46*, 299−329.
Salemme, F. R., Freer, S. T., Xuong, N. H., Alden, R. A., & Kraut, J. (1973) *J. Biol. Chem. 248*, 3910−3921.
Schechter, E., & Saludjian, P. (1967) *Biopolymers 5*, 788−790.
Schellman, J. A. (1978) *Biopolymers 17*, 1305−1322.
Shakhnovich, E., Abkevich, V., & Ptitsyn, O. B. (1996) *Nature 379*, 96−98.
Shao, W., Liu, G., & Tang, W. (1995) *Biochim. Biophys. Acta 1248*, 177−185.
Shastry, M. C. R., & Udgaonkar, J. B. (1995) *J. Mol. Biol. 247*, 1013−1027.
Shastry, M. C. R., Agashe, V. R., & Udgaonkar, J. B. (1994) *Protein Sci. 3*, 1409−1417.
Sosnick, T. R., Mayne, L., Hiller, R., & Englander, S. W. (1994) *Nat. Struct. Biol. 1*, 149−156.
Sosnick, T. R., Mayne, L., & Englander, S. W. (1996) *Proteins: Struct., Funct., Genet. 24*, 413−426.
Tanford, C. (1970) *Adv. Protein Chem. 24*, 1−95.
Timasheff, S. N. (1993) *Annu. Rev. Biophys. Biomol. Struct. 22*, 67−97.
Timasheff, S. N., & Arakawa, T. (1988) in *Protein Structure and Function* (Creighton, T. E., Ed.) pp 331−345, IRL Press, Oxford.
Timkovich, R., & Dickerson, R. E. (1976) *J. Biol. Chem. 251*, 4033−4046.
Tsong, T. Y. (1973) *Biochemistry 12*, 2209−2214.
Vanhove, M., Raquet, X., & Frère, J.-M. (1995) *Proteins: Struct., Funct., Genet. 22*, 110−118.
Wand, A. J., Roder, H., & Englander, S. W. (1986) *Biochemistry 25*, 1107−1114.
Zuniga, E. H., & Nall, B. T. (1983) *Biochemistry 22*, 1430−1437.

BI961976K